Journal of Marine Science and Technology

Volume 25 | Issue 2 Article 18

THE RESEARCH ON COMPRESSOR PERFORMANCE DEGRADATION CAUSED BY TIP CLEARANCE ENLARGEMENT DUE TO CORROSION IN MARINE ENVIRONMENTS

Hai-Ou Sun
Harbin Engineering University, Harbin, Heilongjiang, China.

Jing-Yuan Ma
Harbin Engineering University, Harbin, Heilongjiang, China.

Zhong-Yi Wang
Harbin Engineering University, Harbin, Heilongjiang, China., b205030024@126.com

Lei Cao
Harbin Engineering University, Harbin, Heilongjiang, China.

Recommended Citation
Sun, Hai-Ou; Ma, Jing-Yuan; Wang, Zhong-Yi; and Cao, Lei (2017) "THE RESEARCH ON COMPRESSOR PERFORMANCE DEGRADATION CAUSED BY TIP CLEARANCE ENLARGEMENT DUE TO CORROSION IN MARINE ENVIRONMENTS," *Journal of Marine Science and Technology*: Vol. 25: Iss. 2, Article 18.
DOI: 10.6119/JMST-016-1115-2
Available at: https://jmstt.ntou.edu.tw/journal/vol25/iss2/18

THE RESEARCH ON COMPRESSOR PERFORMANCE DEGRADATION CAUSED BY TIP CLEARANCE ENLARGEMENT DUE TO CORROSION IN MARINE ENVIRONMENTS

Acknowledgements

This work was supported by the National Natural Science Foundation of China (grant number 51309063, 51679051); Specialized Research Fund for the Doctoral Program of Higher Education (grant number 20132304120012).

Journal of Marine Science and Technology, Vol. 25, No. 2, pp. 166-177 (2017)
DOI: 10.6119/JMST-016-1115-2

THE RESEARCH ON COMPRESSOR PERFORMANCE DEGRADATION CAUSED BY TIP CLEARANCE ENLARGEMENT DUE TO CORROSION IN MARINE ENVIRONMENTS

Hai-Ou Sun, Jing-Yuan Ma, Zhong-Yi Wang, and Lei Cao

Key words: blade corrosion, numerical simulation, performance degradation, tip clearance.

ABSTRACT

In the marine environment, the corrosion on a compressor blade caused by salt spray severely affects the compressor performance and poses a threat to its operation reliability. This study simulated the corrosion on the blade caused by salt spray by using the static acceleration test, and analyzed the effects of various tip clearances (corresponding to various corrosion periods) on compressor performance and internal flow field through the numerical simulation method. The results revealed that with the increase in corrosion time, the flow rate, pressure ratio, torque, and power of the compressor decreased. The chart of the compressor internal flow indicated the increasing internal loss and decreasing efficiency. On the basis of loss analysis, the binomial relationships between the service time and relative values of total pressure loss and efficiency loss, respectively, were established.

I. INTRODUCTION

As a critical component of gas turbines, a compressor comprises high-speed rotating blades and is primarily used to increase air pressure for the combustion process in the combustion chamber. In the marine environment, the air is moist and contains corrosive salt aerosol. In ships and offshore platforms powered by gas turbines, the compressor blades undergo scouring because of the salt spray and corrosion when operated at a high speed and pressure. After prolonged operation, the compressor blades become deformed and fail to function, increasing the fracture risk (Ebra, 2006; Mokaberi et al., 2015). Therefore, it is particularly crucial to study the effects of salt fog corrosion on gas turbine performance and shelf life. Salt spray corrosion on compressor blades can be divided into two forms according to the corrosion mechanisms: chemical corrosion, which refers to the damage caused by direct chemical action between the metal surface and nonelectrolyte, and electrochemical corrosion, which refers to the damage caused by the electrochemical reaction between the metal and electrolyte (Han, 2014). The chemical corrosion and electrochemical corrosion on the blade surface caused by acidic and corrosive salt air displace the metal on the surface and alter the blade profile (Huo and Sun, 2002). Corrosion comes in two types of effects: it may roughen the blade surface and increase the thickness of the blade boundary layer, and thus alter the flow rate and pressure ratio efficiency, or it may increase the blade clearance, causing a flow chaos at the blade tip clearance. These effects increase the compressor internal loss and reduce the compressor performance (Kato et al., 2011). This study examined the effects of tip clearance caused by salt fog corrosion on the compressor performance.

Various studies have investigated the effects of tip clearance on the compressor performance domestic and overseas. Some studies have demonstrated that rotor corrosion is more critical than stator corrosion and has more severe effects on compressor performance (Tarabrin et al., 1996; Syverud et al., 2007; Linden, 2011). Denton (1993) identified that complex flow in the tip clearance is the main factor of compressor performance degradation. Wellborn and Okiichi (1999) examined the effects of tip clearance on a multistage axial compressor through experimental analysis and numerical calculation, and the results revealed a 1% decrease in efficiency with 1% tip clearance increase in blade height. More recently, Luo et al. (2015) demonstrated that the increase in tip clearance alters the flow field structure of the upper channel of the rotor blade lattice and rapidly increases the entropy production. Lv et al. (2011) reported that the leakage loss related to blade tip clearance accounts for approximately one-third of the total compressor performance loss. The blade tip clearance modified not only the blade cascade internal flow field but also the air inlet conditions; in short, it affected the whole performance level. However, studies on the relationship between the degree of corrosion and compressor

Paper submitted 12/31/15; revised 06/06/16; accepted 11/15/16. Author for correspondence: Zhongyi Wang (e-mail: b205030024@126.com).
Harbin Engineering University, Harbin, Heilongjiang, China.

Table 1. Various corrosion times corresponding to tip clearance value.

Number	Corrosion time/day	Material loss/g	Material thick loss /mm	Tip clearance /mm
Tip 1	0	0	0	0.51
Tip 2	13	0.025	0.0198	0.67
Tip 3	26	0.085	0.0657	1.03
Tip 4	39	0.23	0.183	1.51
Tip 5	52	0.27	0.212	2.17
Tip 6	65	0.34	0.279	2.77

service time are limited.

In this study, a salt spray test was conducted under laboratory conditions on a compressor blade made of X20Cr13 martensitic stainless steel. During salt spray periods of 13, 26, 39, 52, and 65 days, the sample weight loss was measured using an electronic balance. We assumed that blade weight loss caused by the material corrosion all concentrated in the blade tip. NASA Stage 67 has been extensively studied and has been developed according to the requirements of a typical aero engine high-pressure compressor (Van Zante et al., 2002; Fidalgo et al., 2012). The effects of various tip clearances corresponding to various corrosion degrees on the compressor performance were investigated using NUMECA software, and the formula of the relationship between the compressor service time and loss coefficient was established as the basis for determining compressor corrosion failure.

II. EXPERIMENTAL METHOD

1. Salt Spray Experiment

In this study, the salt spray simulation experiment was performed in a laboratory to mimic the corrosion behavior of X20Cr13 martensitic stainless steel in a marine atmospheric environment. The following test conditions were applied: salt solution mass concentration, 5% ± 0.1%; pH, 6.5-7.2; test chamber temperature, 35°C ± 2°C; sample laying angle, 60°; and salt fog sedimentation rate, 1-2 mL/(80 cm^2h). After the corrosion test, the solution for removing the corrosion product was prepared and used according to the GB/T 16545-1996 standard. The corrosion products on the sample surface were removed using an ultrasonic container in the temperature range of 20°C-25°C. Subsequently, the sample surfaces were washed using distilled water and dried. Finally, the corrosion pit morphology, quantity, area, distribution, and depth were observed under the Leica DMILM (Qingdao top chemical products import & Export Co., Ltd, Qingdao City, Shandong Province, China) microscope and the data were recorded.

2. Relationship Between Weight Loss and Tip Clearance

1) Weightlessness Formula

The sample weight was measured using weighing scales before and after the salt spray test. The weightlessness of the samples could be obtained using the following:

$$\text{Weight loss} = m_0 - m \tag{1}$$

where m_0 is the weight before the salt spray test, and m is the weight after the test.

2) Tip Clearance Formula

With the increase in the salt spray corrosion period, material loss gradually increased and resulted in direct weight loss. According to one previous study, in addition to the increase in damage on the compressor blade surface after long-term operation, the increase in the tip clearance was another crucial factor (Syverud et al., 2007). Moreover, the material loss of the blade tip directly led to an increase in blade tip clearance. Thus, it was assumed that the blade material loss occurred mainly in the compressor blade tip, which led to an increase in blade tip clearance. In addition, the weight loss observed during the salt spray test can be considered a compressor blade material loss, and the relationship between the blade tip clearance and blade weight loss can be calculated using these data. In this study, the X20Cr13 martensitic stainless steel weight loss data obtained during the salt spray test were converted to the tip clearance increase data, as summarized in Table 1.

III. MODEL DESCRIPTION

1. Turbulence Model

The internal flow of the NASA Stage 67 model in this study was the viscous compressible gas flow. The equations of continuity, momentum, and energy of this flow are as follows:

$$\frac{\partial \rho}{\partial t} + \nabla \cdot (\rho \vec{v}) = 0 \tag{2},$$

$$\frac{\partial}{\partial t}(\rho \vec{v}) + \nabla \cdot (\rho \vec{v}\vec{v}) = \nabla \cdot (-pI + \Gamma) \tag{3},$$

$$\frac{\partial}{\partial t}(\rho E) + \nabla \cdot (\rho \vec{v} E) = \left[(-pI + \Gamma) \cdot \vec{v}\right] - \nabla \cdot \vec{q} \tag{4},$$

where $I = \{\delta_{ij}\}$ is the unit tensor and $\Gamma = \{\tau_{ij}\}$ is the viscous stress tensor term, which is defined as follow:

$$\tau_{ij} = \frac{2}{3}\mu \frac{\partial u_k}{\partial x_k}\delta_{ij} + \mu\left(\frac{\partial u_i}{\partial x_j} + \frac{\partial u_j}{\partial x_i}\right) \tag{5}.$$

Table 2. Computational grid.

Object	Length-width ratio	Ductility ratio	Orthogonality	Grid number
Rotor	1858	4	18.4	1800000
Stator	1300	3	40.7	1000000

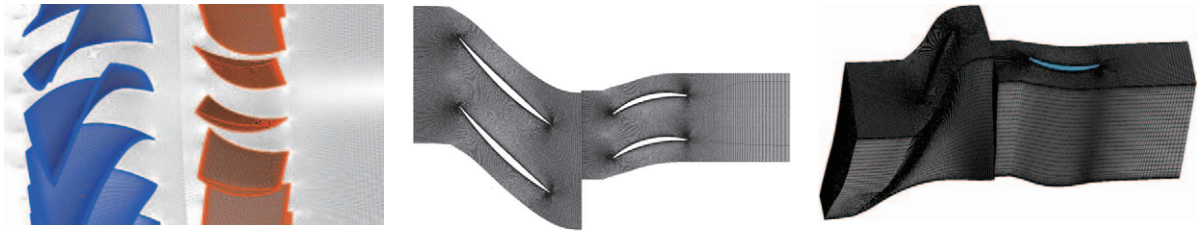

(a) Blade mesh (b) Cross-section grid of 50% blade height (c) Single-channel calculation domain model

Fig. 1. Grid diagram.

Furthermore, $\vec{q} = \{q_i\}$ represents the heat flux and E is the total energy per unit mass of fluid, which are expressed as follows:

$$\vec{q} = K\nabla \cdot T \tag{6},$$

$$E = e + \frac{1}{2}\vec{v}\cdot\vec{v} \tag{7},$$

where E is the total energy of the fluid, e the internal energy per unit fluid, $\vec{v}$ the velocity vector, K is the heat transfer coefficient, and T is the temperature.

The above equation is the famous Navier-Stokes equation, which ignores gravitational force. To complement the information obtained from the preceding equations, this study combined the gas pressure with density using the compressible gas state equation. The relationship is presented as follows:

$$\frac{P}{\rho} = RT \tag{8}.$$

Additionally, the fluid viscosity coefficient μ is related to the temperature T; the Sutherland formula is also often used in engineering to determine the value of the fluid viscosity coefficient, which is given as follows:

$$\frac{\mu(T)}{\mu_0} = \left(\frac{T}{T_0}\right)^{3/2} \frac{(T_0 + T_S)}{(T + T_s)} \tag{9}$$

where T_0 = 293.15 K, T_s is the Sutherland constant, μ_0 is the viscous coefficient of gas at temperature T_0, the value 1.716 × 10^{-5} Pa·s.

The standard κ – ε turbulence model is widely applied for computational simulation in the existing turbulence models (Jones and Launder, 1972). Featured with better stability, higher calculation accuracy, and faster calculation convergence, the standard κ – ε turbulence model can be more efficiently applied to some complex flow calculations and is more widely used in turbulence research. This study selected the standard κ – ε turbulence model to numerically simulate various operating conditions of the compressor by considering the characteristics of the compressor's internal flow field and the computational grid requirements of various turbulence models.

2. Mesh Generation and Boundary Conditions

1) Mesh Generation

Structured grids were generated using the Autogrid 5 module in the NUMECA software. The areas around the blade were discretized into the O-type grid, the import and export areas and far wall part were discretized into the H-grid, the tip clearance was discretized into the butterfly grid (to improve grid quality), and the near wall part grid was refined. Fig. 1 depicts the grid diagram and Table 2 presents the grid quality, which met the computational requirements.

2) Boundary Conditions

The boundary conditions were as follows:

Inlet: axial flow direction, total temperature = 288.15 K, total pressure = 101,325 Pa.
Outlet: pressure outlet, static pressure obtained using the radial equilibrium equation, average radius = 0.187 m, reference pressure = 101,325 Pa.
Solid wall: adiabatic, no slip.

The compressor characteristic curve was calculated at four speeds: 100% design speed at 16,043 r/min, 90% design speed at 144,387 r/min, 80% design speed at 12,834 r/min, and 70% design speed at 11,230 r/min. Notably, the convergence criteria for these computations were based on the reduction of root mean

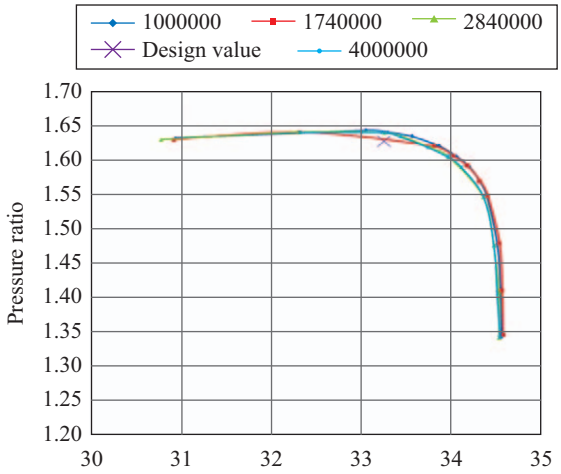

(a) Total pressure ratiocurve with various numbers of gridcomputing

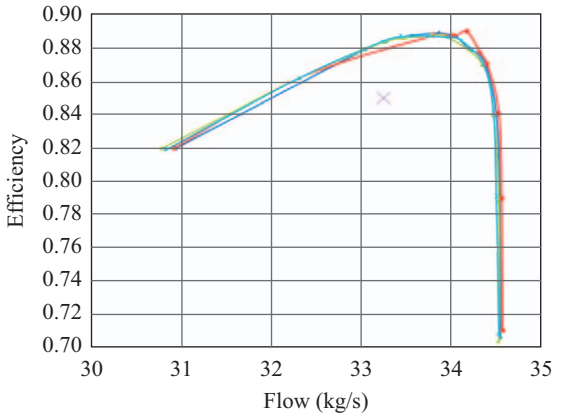

(b) Efficiencycurve with various numbers of grid computing

Fig. 2. Grid independence test results.

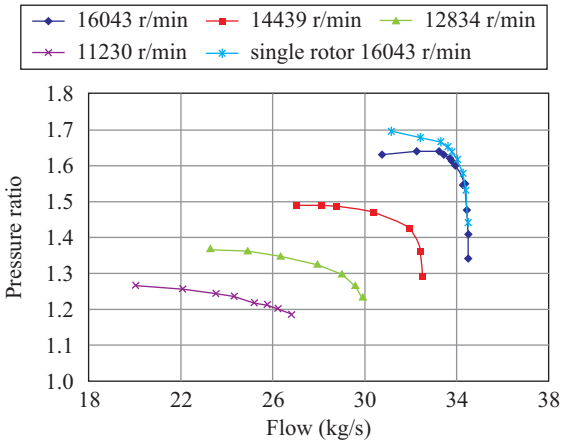

(a) Characteristic curves of compressor pressure ratios under various rotational speeds

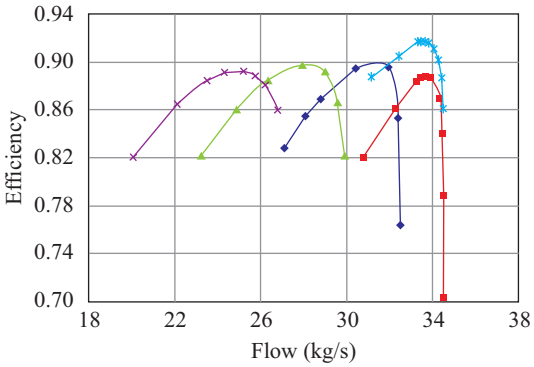

(b) Compressor efficiency characteristic curve under various rotational speeds

Fig. 3. Compressor characteristic curves under various speed conditions.

square (RMS) residuals below 1×10^{-6}.

3. Calculation Model and Validation

1) Testing and Verifying Grid Independence

The number of grids used in the grid independence test was 1, 1.7, 2.8 and 1.7 million. According to the calculation results depicted in Fig. 2, the computation results of various numbers of grids exhibited similar changing trends, whereas the curves of the computed results slightly varied. Among them, the curves of 2.8 million and 4 million grids almost entirely overlapped.

2) Model Validation

Fig. 3 illustrates the compressor performance curves of the NASA Stage 67 at speeds of 100% (16,043 r/min), 90% (14,439 r/min), 80% (12,834 r/min), and 70% (11,230 r/min), and Table 3 presents the contrast between the simulation and design values. Notably, the difference between the simulation and design values was at most 5%; therefore, the model was effective and could be used for the calculation.

IV. RESULTS AND DISCUSSION

1. Flow

The effects of rotor blade tip clearance on the turbine performance were evaluated. To quantitatively analyze the effects of blade tip clearance size on compressor flow, the statistics of flow recession conditions corresponding to the peak efficiency points with five tip clearances and at four rotational speeds were obtained (Table 4), with the blade data corresponding to the design tip clearance data used as the reference value. The flow recession formula is as follows:

$$\text{Flow recession} = (F_1 - F_n)/F_1 \qquad (10),$$

where F_1 is the flow of Tip 1 and F_n is the flow of the nth tip ($n = 2 - 4$). The recession formulas of relative parameters, such as pressure ratio and efficiency, were similarly derived in this study.

Table 4 reveals that flow recession caused by tip clearance was higher at a high speed than a low speed. Moreover, the higher the blade tip clearance value, the higher the amount of recession.

Table 3. Contrast between simulation and design values.

(a) Contrast between single-rotor simulation value and design value

Performance parameter	Design value	Simulation value	Error %
Overall pressure ratio	1.64	1.66	0.7313
Isentropic efficiency %	92.0	91.6	0.4
Flow	33.25	33.63	1.1

(b) Contrast between whole-level simulation value and design value

Performance parameter	Design value	Simulation value	Error %
Overall pressure ratio	1.64	1.63	0.73
Isentropic efficiency %	85.0	88.7	4.17
Flow	33.25	33.70	1.3

Table 4. Statistics of compressor flow recession corresponding to the peak efficiency point under various rotation speeds.

Number	100% rotate speed		90% rotate speed		80% rotate speed		70% rotate speed	
	Flow/kg/s	Recession/%	Flow/kg/s	Recession/%	Flow/kg/s	Recession/%	Flow/kg/s	Recession/%
Tip 1	33.76	-	31.96	-	27.95	-	25.25	-
Tip 2	33.67	0.26	31.92	0.10	27.91	0.14	25.21	0.15
Tip 3	33.45	0.90	31.73	0.72	27.80	0.55	25.12	0.49
Tip 4	32.94	2.44	31.47	1.52	27.63	1.14	24.99	1.00
Tip 5	32.36	4.15	31.12	2.61	27.38	2.05	24.83	1.65
Tip 6	32.17	4.71	30.76	3.73	27.11	3.01	24.66	2.33

Table 5. Average recession of compressor efficiency and pressure ratio (%).

Tip clearance/mm		0.67	1.03	1.51	2.17	2.77
Efficiency average recession	100% rotate speed	0.160	0.640	1.654	2.144	2.549
	90% rotate speed	0.367	0.394	0.815	1.306	1.894
	80% rotate speed	0.191	0.458	0.691	1.177	1.673
	70% rotate speed	0.148	0.329	0.557	0.871	1.258
Pressure ratio average recession	100% rotate speed	0.044	0.232	0.467	2.307	3.278
	90% rotate speed	0.123	0.142	0.293	0.506	0.712
	80% rotate speed	0.102	0.183	0.287	0.457	0.630
	70% rotate speed	0.019	0.064	0.129	0.220	0.325

2. Pressure Ratio and Efficiency

Table 5 presents the statistics of efficiency and pressure ratio recession as they correspond to the peak efficiency points with five tip clearances and four rotational speeds. At a constant tip clearance, the recession of compressor efficiency and pressure ratio at a high speed was relatively large. At a constant speed, the higher the tip clearance was, the higher the performance decline was. Thus, blade corrosion had a substantial influence on the overall performance of the compressor. For example, when the blade tip clearance value was 2.77 mm (5.4 times the design clearance value), the efficiency recession reached 2.549% and the pressure ratio recession reached 3.278% at 100% speed.

3. Torque and Power

A list of the statistics of recession of torque and power conditions as they correspond to the peak efficiency points with five tip clearances and four rotational speeds is presented in Table 6. In short, the torque and power of the compressor demonstrated a recession when the tip clearance increased, and the recession increased when the corresponding tip clearance increased. However, the formation of the tip clearance vortex and the enhancement of leakage flow may have also led to the increase in compressor loss because of the increase in tip clearance. Thus, the flow simultaneously became unstable and resulted in torque recession.

4. Inner Flow Analysis

1) Mach Number Distribution

Fig. 4 presents the Mach number distribution of the cross-

Table 6. Average recession of compressor torque and power (%).

Tip clearance/mm		0.67	1.03	1.51	2.17	2.77
Torque average recession	100% rotate speed	2.971	3.413	4.056	5.347	8.030
	90% rotate speed	0.290	0.520	1.340	2.468	3.654
	80% rotate speed	0.264	0.648	1.246	2.445	3.312
	70% rotate speed	0.533	0.931	1.629	2.335	3.231
Power average recession	100% rotate speed	0.323	3.413	4.056	5.347	8.030
	90% rotate speed	0.043	0.072	0.318	0.587	0.615
	80% rotate speed	0.010	0.067	0.101	0.274	0.276
	70% rotate speed	0.410	0.369	0.113	0.149	0.149

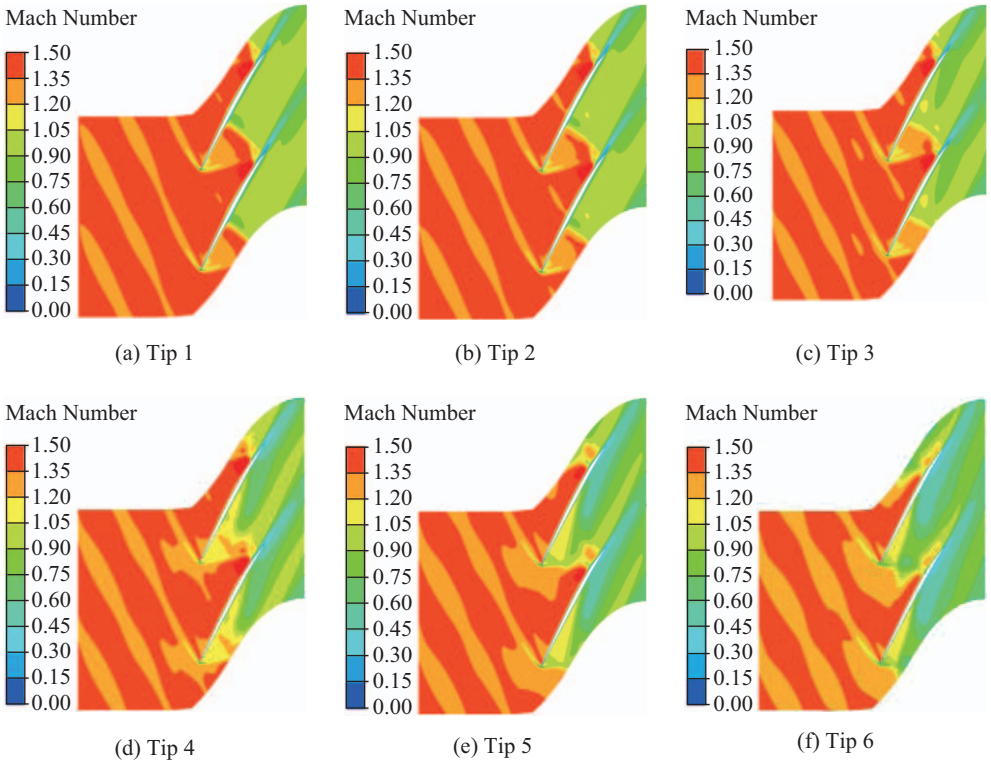

Fig. 4. Mach number distribution of the dynamic blade cross section, corresponding to peak efficiency points at the 95% high position.

section of the dynamic blade corresponding to peak efficiency points in six calculation models at the 95% high position. The Mach number of the suction surface leading edge in the blade passage and the front of the blade passage was approximately 1.4, whereas the Mach number of the trailing edge area was approximately 0.8 and exhibited a uniform distribution. Only a small range of low velocity regions was observed at the wake regions of the blade.

Compared with the results presented in Fig. 6, the Mach number distribution in the whole flow field changed slightly with the increase in tip clearance. The main difference was that the high Mach number region moved toward the leading edge along the suction surface, whereas the scope became narrow. Moreover, the relative Mach number region with low values continued to expand with the increase in tip clearance, whereas the lowest relative Mach number value gradually decreased simultaneously. However, the low-value region approached the high-value region to change the shape of the high-value region, and gradually approached the pressure surface of the adjacent blade. Therefore, the high- and the low-value regions accounted for almost the entire S1 stream surface with 5% chord length clearance, which had a considerable effect on the compressor aerodynamic performance. Notably, Yamada et al. (2011) analyzed the characteristics of the compressor performance in the same area.

2) Total Pressure Distribution

Fig. 5 depicts the total pressure distribution in the dynamic blade cross section, corresponding to peak efficiency points at the 95% high position. Specifically, a low-pressure region

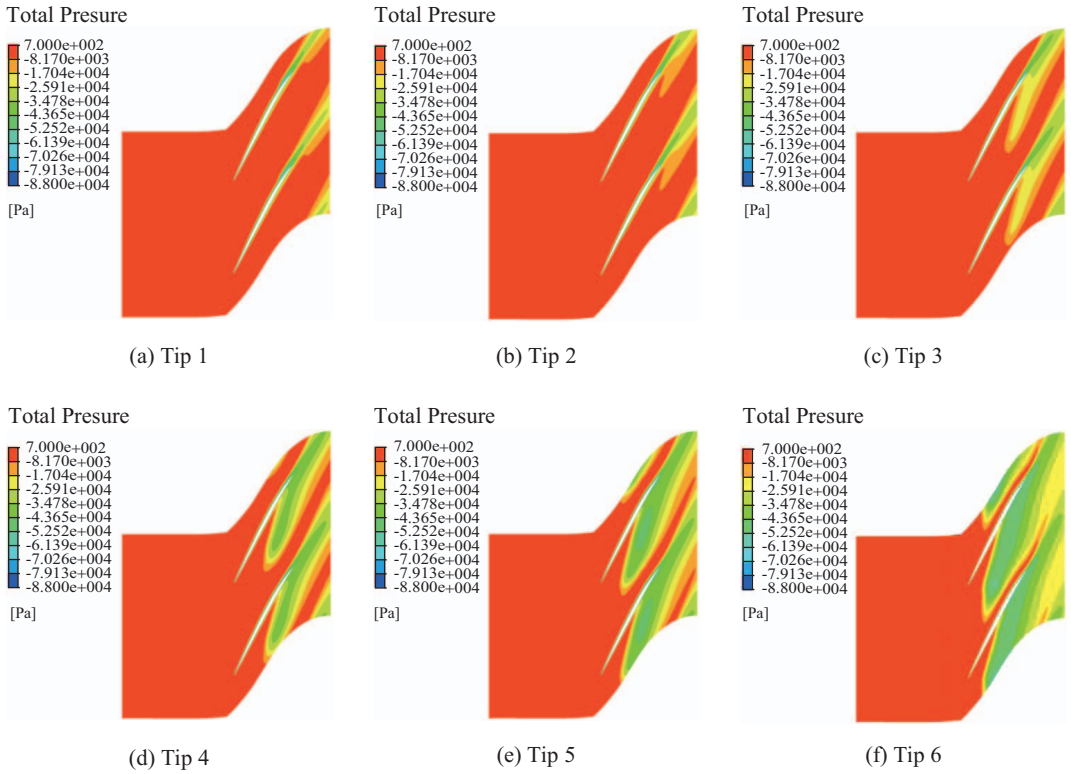

Fig. 5. Total pressure distribution of the dynamic blade cross section, corresponding to peak efficiency points at the 95% high position.

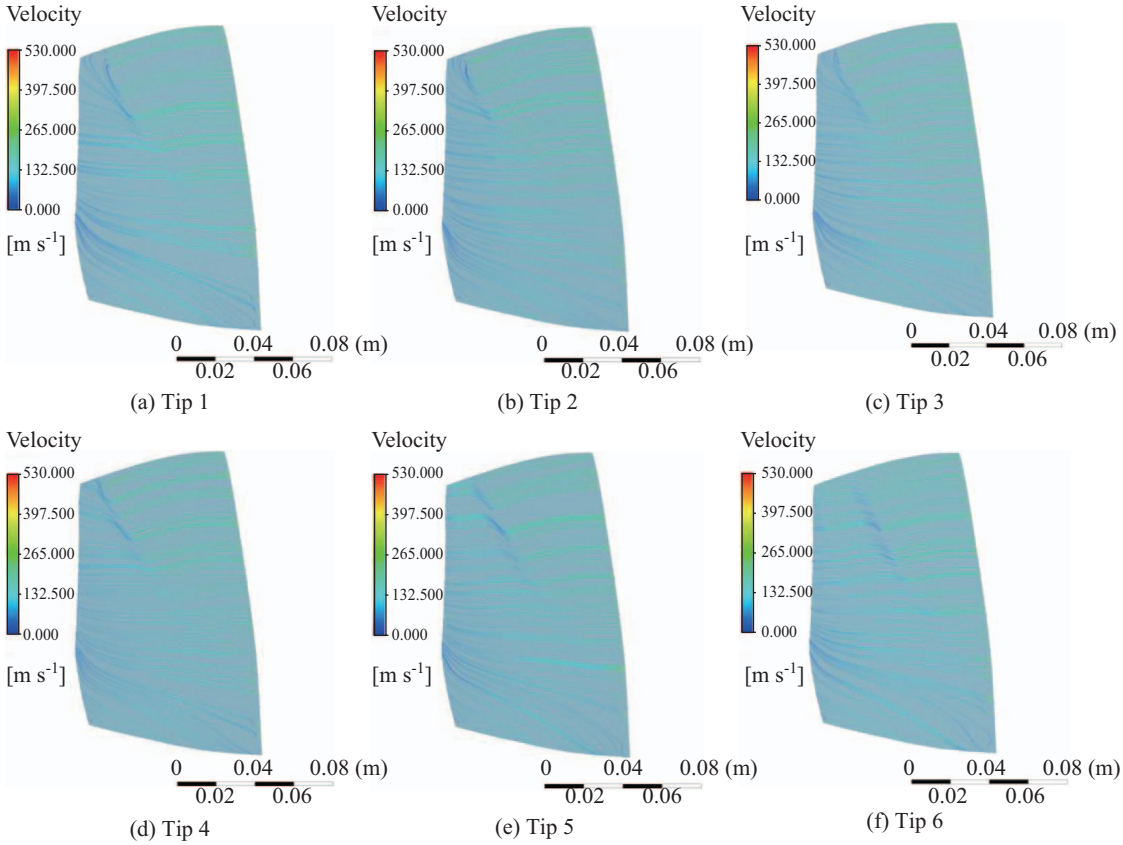

Fig. 6. Limited streamlines of dynamic blade suction surface corresponding to peak efficiency points.

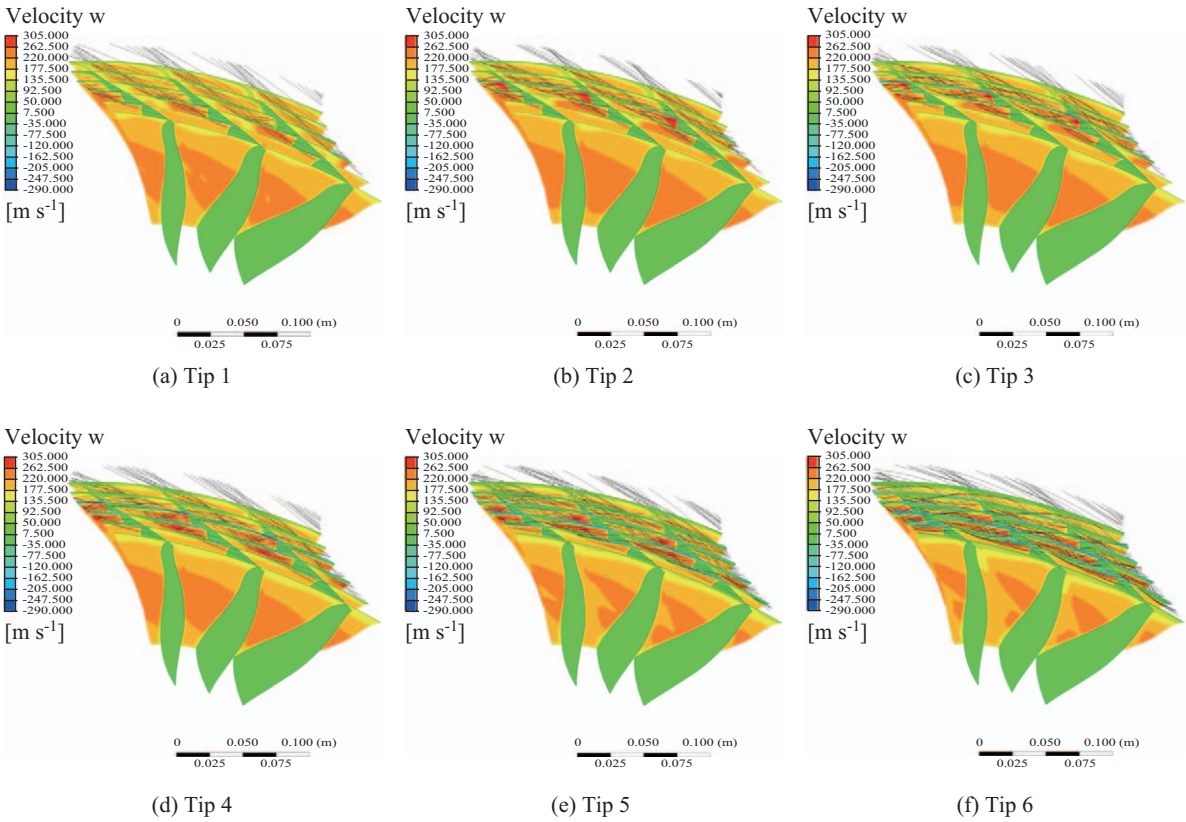

Fig. 7. Relative velocity distribution of the equal chord length cross section of the blade passage and blade tip streamlines that correspond to peak efficiency points.

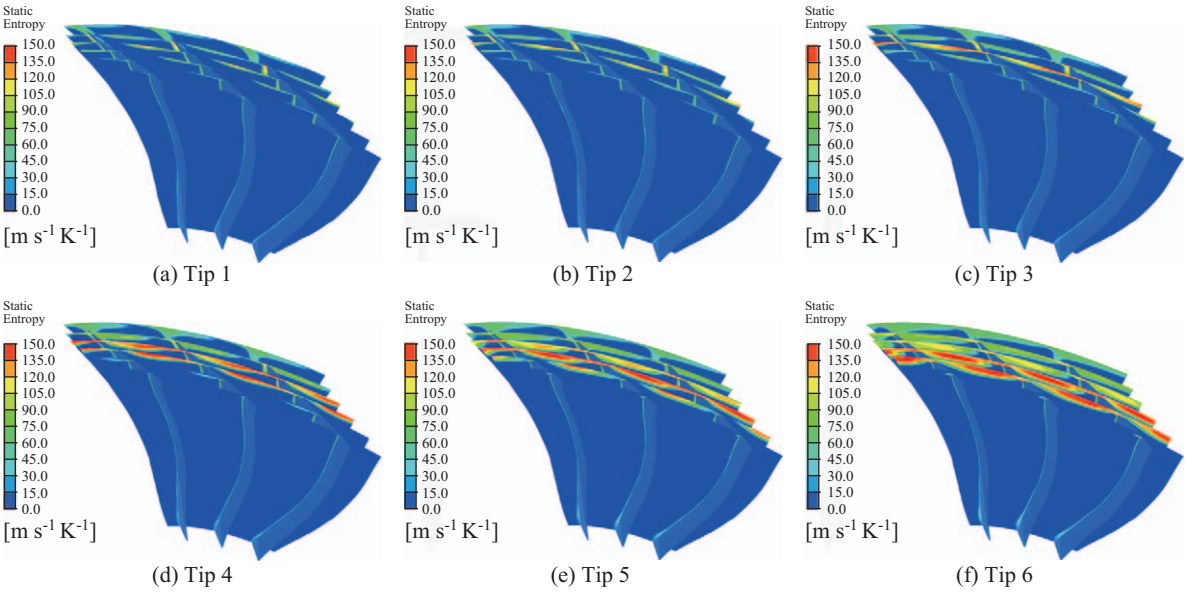

Fig. 8. Static entropy distribution of the equal chord length cross section of the blade passage and blade tip streamlines that correspond to peak efficiency points.

emerged on the suction side near the trailing edge, and a high range of low-pressure region emerged on the pressure side near the trailing edge. Two pressure regions then formed because of the flow separation effect on the suction side and tip clearance leakage flow. The pressure gradient on both sides of the blade allowed a considerable amount of fluid to pass through

the tip clearance and continually flow back to the low-pressure region of the blade from the high-pressure region of the blade basin. This is the main reason for the clearance leakage flow. With the increase in tip clearance, clearance leakage exerted a higher effect on the pressure distribution of the S1 stream surface. The low-pressure region values near the pressure side decreased but the scope gradually expanded. This can be explained by the finding that more fluid passed the tip clearance and was lost from the pressure surface. Therefore, the scope of the low-pressure region near the trailing edge of the suction surface expanded, whereas the minimum static pressure value continuously decreased. This indicated that the strength of clearance leakage was substantially enhanced when the clearance was large, and thus, the flow loss also significantly increased. Meanwhile, a leakage flow formed in the low-pressure region, which had an effect on the scope and size of the low-pressure region and ultimately affected compressor performance. Moreover, research by Zhang et al. (2014) demonstrated that the leakage flow had a certain effect on the pressure and the performance of the compressor.

3) Limiting Streamlines of the Rotor Blade Suction Side Surface

Fig. 6 presents the limiting streamlines of the dynamic blade suction surface corresponding to peak efficiency points in six calculation models. An obvious separation was observed, which extended from the blade root of the leading edge on the suction surface to the trailing edge of the blade tip. In addition, an obvious separation vortex was observed at the trailing edge of the blade root on the suction surface. As outlined in Fig. 6, the flow separation region expanded significantly and the separation start point at the blade root moved to the trailing edge, whereas the separation start point in the blade tip position moved forward substantially with the increase in tip clearance. Moreover, the separation vortex at the blade tip position gradually expanded, indicating that the flow condition of the compressor blade surface changed substantially with the increase in tip clearance and higher leakage flow. The severe separation increased the losses in the compressor stage and reduced the efficiency. Notably, this finding is consistent with that from a study by Wu et al. (2012).

4) Relative Velocity Distribution and Tip Flow Streamlines

Fig. 7 illustrates the relative velocity distribution of equal chord length across the section of the blade passage and blade tip streamlines that correspond with peak efficiency points. The leakage vortex appears in the leading edge of rotor blade and is constantly developing to backside. With the constant enlargement of the tip clearance, the streamline space position was altered slightly in the flow field and only slightly moved toward the blade suction surface. Notably, the streamline was chaotic, which indicated that the mixture between the leakage vortex and surrounding flow strengthened continuously.

Subsequently, as depicted in Fig. 7, the relative velocity on the surface of the S3 changed slightly and the relative velocity along the streamline direction first passed a high-speed region and then rapidly declined and expanded to a low-speed region. The high-speed region was formed because of the flow jet through a small tip clearance under the pressure difference between the suction surface and pressure surface to obtain a higher speed than that of the surrounding fluid. However, with the continuous mixing of the leakage vortex and the surrounding fluid, the loss increased and the relative speed rapidly decreased to a level lower than that of the surrounding fluid. Therefore, a low-speed region was formed behind the streamline. With the increase of the tip clearance, the low-speed region appeared and expand. The low-speed region from scratch to continuously expand with the expansion of the blade tip clearance, which leads to both the expansion of the leakage vortex volume and substantially low energy flow at a low speed in the middle of the flow field. In short, the flow field demonstrated an obvious blocking effect (Lu et al., 2014).

5) Static Entropy Distribution

Fig. 8 presents the static entropy distribution of equal chord length across the blade passage section and blade tip streamlines that correspond to the peak efficiency points. The static entropy of the leakage vortex was higher than that of the surrounding flow field, indicating air had mixed in the leakage vortex. The influence range of the entropy gradually increased with the increase in tip clearance, suggesting an increase in the volume and leakage vortex strength. The axial distribution of maximum entropy expanded from approximately 70% chord to approximately 30% chord. This indicates that the leakage vortex core along the streamline expanded from the trailing edge of the dynamic blade to the leading edge. Furthermore, the entropy increase represented an increase in loss that corresponded to the position and scope of the leakage vortex. Notably, Duan et al. (2012) obtained similar results in their analysis.

5. Loss Analysis

1) Pressure Coefficient

Fig. 9 outlines the pressure coefficient curves of the dynamic blade at the 50% high position, corresponding to the peak efficiency points in six calculation models. The effect of tip clearance variation on the blade surface pressure distribution depends on the pressure surface leading edge to the 50% axial chord length region, as well as the suction surface of the chord length region. Overall, the effect on the pressure surface trailing edge region was relatively small. Suction surface between 30% and 65% of axial chord length region had a larger adverse pressure gradient, and the boundary layer separation is more likely to occur with a larger adverse pressure gradient. With the increase in tip clearance, the pressure coefficient also increased and the start position of separation gradually moved to the leading edge, which is characteristic of the enhancement of the blade suction surface separation region and forward movement of the separation point. With the increase in tip clearance near the pressure surface leading edge, the blade load suddenly increased, leading

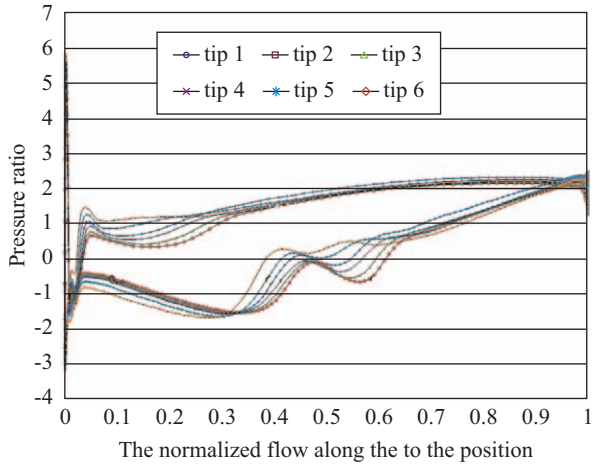

Fig. 9. Pressure coefficient curve at 50% of the height rotor, corresponding to peak efficiency points.

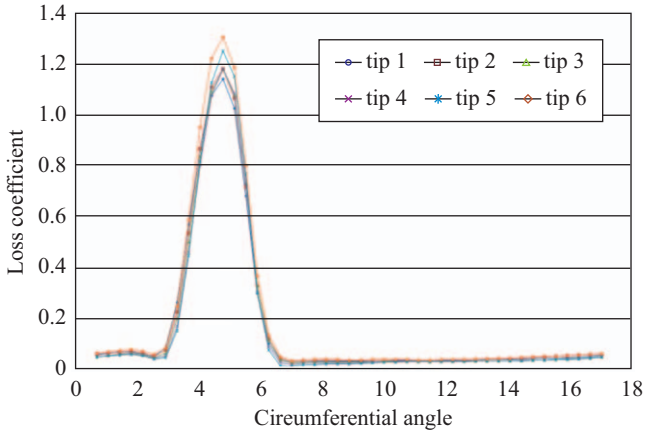

Fig. 10. Circumferential distribution of loss coefficient as 102% of the axial chord length rotor at 50% blade height position, which corresponds to peak efficiency points.

to a small scale of air separation in the front. Because of the separation of the pressure surface leading edge and the increase in the mixing loss of the trailing edge caused by the suction surface separation, the efficiency of the compressor noticeably decreased.

2) Loss Coefficient

Fig. 10 presents the circumferential distribution of the loss coefficient Y_p as 102% of the axial chord length dynamic blade at 50% blade high position. The loss coefficient directly reflects the total pressure loss in the flow field, which gradually increased to a peak in the range of 3°-7°, and then subsequently decreased. It also corresponds to the region where the boundary layer flow and separation flow mixed with the mainstream most strongly in the trailing edge position after the air passed a blade. Moreover, it is the region with maximum total pressure loss. Overall, the loss coefficient peak value increased with an increase in tip clearance because of the enlargement of the blade suction surface region. The strength of leakage flow increased accordingly, resulting in higher energy loss. Additionally, the increase in blade tip clearance in the mainstream of the blade passage region had a minimal impact on the loss coefficient, and thus can be ignored.

3) Total Loss Coefficient and Efficiency Loss Coefficient

Finally, the friction loss of the boundary layer gas and the expansion of the suction surface separation region led to an increase in separation loss with the increase in blade roughness. Therefore, the efficiency, pressure ratio, and flow of the compressor decreased. The loss at the stage was generally expressed by the total loss coefficient ϖ, which includes both blade profile loss and shock loss. The total loss coefficient of the NASA Stage 67 rotor is defined as follows:

$$\varpi = \frac{\left(P'_{ideal}\right)_{te} - P'_{te}}{P'_{le} - p_{le}} \approx \frac{P'_{le} - P'_{te}}{P'_{le} - p_{le}} \qquad (11),$$

where superscript $'$ represents the parameters of the relative dynamic blade, subscripts *le* and *te* denote the leading edge and trailing edge, respectively, and P and p are the total pressure and static pressure, respectively. Because the total pressure of an ideal process cannot be determined, the total pressure of the leading edge was approximately equal to the total pressure of the trailing edge of the ideal process.

The effect of surface roughness on the compressor efficiency parameter was expressed using the efficient loss coefficient ζ as follows:

$$\zeta = 1 - \eta_{is} \qquad (12).$$

According to the definition of the total loss coefficient ϖ and efficiency loss coefficient ζ, the calculated peak efficiency points for various roughness values of the dynamic blade were treated as a reference operation. Table 7 presents the calculation results. In short, the total loss coefficient and efficiency loss coefficient of the entire stage compressor increased with an increase in tip clearance. Figs. 11 and 12 depict the polynomial curve of the relationship between service time and the relative value of the total loss coefficient ϖ and efficiency loss coefficient ζ, respectively, which are based on the calculation results under the design clearance. Using Eqs. (13) and (14), the fitting R2 values of the total loss coefficient and efficiency loss coefficient were determined to be 0.9919 and 0.9709, respectively. This indicates that the fitting formula and data, as well as the credibility of the formula, are efficient.

$$\frac{\varpi}{\varpi_{smooth}} = 0.0228 \times Y^2 - 0.0436Y + 1.0079 \qquad (13)$$

and

$$\frac{\zeta}{\zeta_{smooth}} = 0.0051 \times Y^2 - 0.0140Y + 1.0026 \qquad (14).$$

Table 7. Parameter calculation results under peak efficiency points.

Number	Tip clearance/mm	Corrosion test/day	Service time/year	ϖ	ζ
Tip 1	0.51 (design value)	0	0	0.1879	0.1136
Tip 2	0.67	13	1	0.1878	0.1174
Tip 3	1.03	26	2	0.1918	0.1180
Tip 4	1.51	39	3	0.1991	0.1227
Tip 5	2.17	52	4	0.2266	0.1317
Tip 6	2.77	65	5	0.2557	0.1353

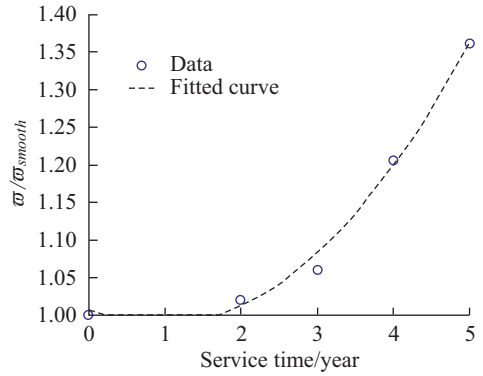

Fig. 11. Polynomial curve of the relationship between service time and the relative value of the total loss coefficient.

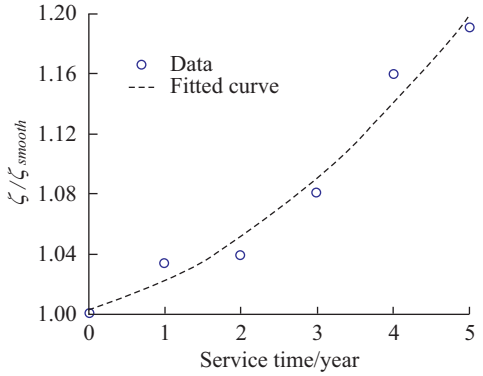

Fig. 12. Polynomial curve of the relationship between service time and the efficiency loss coefficient.

V. CONCLUSIONS

This study established the relationship between the material weight loss and tip clearance variation on the basis of corrosion test data. The weight loss data obtained from the test were reduced to the blade wear material loss and the change in the blade tip clearance value was obtained. Six calculation models were presented, and generated their corresponding mesh to perform calculations at multiple speeds and under various conditions. The effect of the change in blade tip clearance on the overall performance of the compressor was analyzed at various tip clearance values, corresponding to the compressor aerodynamic characteristics. Referring to the analysis of internal flow characteristics, the influence regularity of the blade tip clearance variations on the internal flow of the compressor was summarized. Finally, the functional relationship of the loss characteristic under the compressor service life was obtained using this scheme.

ACKNOWLEDGEMENTS

This work was supported by the National Natural Science Foundation of China (grant number 51309063, 51679051); Specialized Research Fund for the Doctoral Program of Higher Education (grant number 20132304120012).

REFERENCES

Chinese national standard. Corrosion of metal and alloy-corrosion product removal (GB/T 16545-1996).

Denton, J. D. (1993). Loss mechanism in turbomachines. Journal of Turbomachinery 115, 621-656.

Duan, Z., Y. Liu and L. Lu (2012). Numerical investigation of the behavior of tip leakage flow in a low-speed axial compressor rotor at near-stall condition. Turbine Technical Conference and Exposition 8,461-471.

Ebra, R. (2006). Corrosion fatigue phenomena learned from failure analysis. Engineering Failure Analysis 13, 516-525.

Fidalgo, V. J., C. A. Hall and Y. Colin (2012). A Study of fan-distortion interaction within the NASA dRotor 67 transonic stage. The American Society of Mechanical Engineers 134(5).

Han, G. (2014). Salt fog corrosion prevention of metal equipment. China Science And Technology Information 19, 147-148.

Huo, W. and H. Sun (2002). Corrosion and precaution for blades of aero-engine compressor in the navy air arm. Aviation Engineering and Maintenance, 39-41.

Jones, W. P. and B. E. Launder (1972). The prediction of laminarization with two equation model of turbulence. International Journal of Heat and Mass Transfer 15, 301-314.

Kato, H., H. Taniguchi, K. Matsuda, K. Funazaki, D. Kato and G. Pallot (2011). Experimental and numerical investigation on compressor cascade flows with tip clearance at a low Reynolds number condition. Thermal Science 20, 481-500.

Linden, D. (2011). Long term operating experience with corrosion control in industrial axial flow compressors. Proceedings of the fortieth turbomachinery symposium, 93-106.

Lu, X., W. Chu and J. Zhu (2006). Mechanism of the interaction between casing treatment and tip leakage flow in a subsonic axial compressor. Power for Land, Sea, and Air 6,79-90.

Luo, X., Y. Yu and Y. Li (2015). Numerical simulation of effects of tip clearance on axial compressor aerodynamic performance. Thermal Turbine 44, 62-67.

Lv, Z., X. Liu and Y. Feng (2011). Numerical study of effect on different tip caps in a three and a half stages compressor. Steam Turbine Technology 53, 429-432.

Mokaberi, A., R. Derakhshandeh-Haghighi and Y. Abbaszadeh (2015). Fatigue

fracture analysis of gas turbine compressor blades. Engineering Failure Analysis 58, 1-7.

Syverud, E., O. Brekke and L. E. Bakken (2007). Axial compressor deterioration caused by saltwater ingestion. American Society of Mechanical Engineers 129, 119-127.

Tarabrin, A. P., V. A. Schurovsky, A. I. Bodrov and J.-P. Stalder (1996). An analysis of axial compressors fouling and a cleaning method of their blading. American Society of Mechanical Engineers, 96-GT-363.

Van Zante, D. E., W.-M. To and J.-P. Chen (2002). Blade row interaction effects on the performance of a moderately loaded NASA transonic compressor stage. The American Society of Mechanical Engineers 5, 969-980.

Wellborn, S. R. and T. H. Okiishi (1999). The influence of shrouded stator cavity flows on multistage compressor performance. Journal of Turbomachine 121, 486-498.

Wu, Y., Q. Li, J. Tian and W. Chu (2012). Investigation of pre-stall behavior in an axial compressor rotor-Part 1: Unsteadiness of tip clearance flow. ASME 134(5), 051027-051027-12.

Yamada, K., M. Furukawa and H. Fukushima (2011). The role of tip leakage vortex breakdown in flow fields and aerodynamic characteristics of transonic centrifugal compressor impellers. ASME 7, 2111-2123.

Zhang, C., J. Hu and Z. Wang (2014). Investigations on the effects of inflow condition and tip clearance size to the performance of a compressor rotor. Journal of Engineering for Gas Turbines and Power 136(12), 122608-1226081-7.